

SYNTHESIS AND CHARACTERIZATION OF γ -Al₂O₃@MgO SORBENT FOR EFFICIENT REMOVAL OF Pb FROM AQUEOUS SOLUTIONS

Kim Thanh Nguyen^{1,*}, Thi Lan Anh Nguyen¹, Minh Tuan Duong¹, Viet Linh Pham¹,
Thi Vinh Hanh Le¹, Van Hao Ha¹, Vu Sinh Tran¹, The Son Le^{1,*}

¹Faculty of Physics and Chemical Engineering, Le Quy Don Technical University, Hanoi, Vietnam

Abstract

This study focuses on enhancing the adsorption capacity for lead ions by introducing MgO onto the surface of γ -Al₂O₃, forming γ -Al₂O₃@MgO. The γ -Al₂O₃ nanoparticles were synthesized via the sol-gel method on a citrate template. MgO was incorporated onto the surface of the γ -Al₂O₃ nanoparticles, with varying MgO concentrations (5%, 10%, and 15% by weight), achieved through the absorption of magnesium ions onto the material's surface followed by sintering at 773K. The findings indicated that both the γ -Al₂O₃ and MgO crystalline phases exhibit a cubic structure (Fd3m symmetry group), which is formed within the sample. Although the specific surface area diminished from 166 m²/g to 135 m²/g, the surface basicity increased proportionally to the amount of MgO incorporated into the sample. The impacts of various adsorption conditions such as pH, adsorbent mass, and contact time on the Pb²⁺ ion adsorption capacity was systematically examined. Optimal conditions (pH = 7, adsorption time of 8 hours) highlighted that the γ -Al₂O₃ material containing 10% MgO by weight showcased the highest Pb²⁺ adsorption capacity at 145 mg/g, surpassing the adsorption capacity of 135 mg/g for the γ -Al₂O₃ material.

Keywords: γ -Al₂O₃@MgO; lead adsorption; basic surface modification.

1. Introduction

Heavy metals represent some of the gravest contaminants in the environment, notably within water and soil systems. Their presence jeopardizes both ecosystems and human health through the food chain. Consequently, it is imperative to establish effective strategies for alleviating heavy metal pollution. The discharge of heavy metals directly into the environment, from wastewater can inflict harm on various life forms [1, 2]. The escalating introduction of heavy metals into water sources has emerged as a significant and worrisome environmental and public health concern due to their toxicity and resistance to biodegradation [2].

* Email: thanhnk@mta.edu.vn; sonlt@lqdtu.edu.vn
DOI: 10.56651/lqdtu.jst.v1.n02.712.pce

Numerous technologies have emerged to address the extraction of toxic heavy metals from wastewater. These encompass methods such as reduction and precipitation [3], coagulation and flotation [4], adsorption [5, 6] ion exchange, membrane techniques, and electrolysis [7]. However, these techniques tend to be either costly or ineffective, particularly when dealing with metal concentrations exceeding 100 ppm [8]. Among these approaches, adsorption has emerged as a preferred technique for wastewater treatment due to its cost-effectiveness, wide applicability, efficiency, and limited sludge generation [9, 10]. A notable trend involves exploring unconventional, low-cost materials as adsorbents for heavy metal removal. This encompasses various inorganic and organic adsorbents like zeolites, clay minerals, fly ash, biosorbents, and activated carbon [10, 11]. Additionally, considerable attention has shifted toward employing nanoparticles for heavy metal removal due to their unique attributes such as high adsorption capacities, exposed surfaces, simplified operation, and production feasibility [12, 13]. Recent advancements in nanotechnology have expanded the range of potential adsorbent materials. Various nanomaterials, including carbon nanotubes [14], nanometal oxides [12], and magnetic nanoparticles [13] have recently emerged as potential adsorbents for heavy metals. Among these, metal oxides and their combinations have demonstrated adsorbent potential when appropriately prepared and activated. Magnesium oxide, with its non-toxic, non-corrosive, thermally stable, and environmentally friendly attributes, has gained attention [15, 16]. Nano-alumina, a versatile ceramic material with applications in electronics and catalysis, has shown promise in various chemical reactions and water treatment [17, 18].

This study focuses on development of a sorbent material composing of magnesium oxide (MgO), and commonly used nano-alumina (Al_2O_3). The primary objective of this investigation is to first assess the capacity of $\gamma\text{-Al}_2\text{O}_3$ adsorbent, prepared via the citrate sol-gel method, in adsorbing heavy metal Pb^{2+} ions. Concurrently, we aim to enhance the Pb^{2+} ion adsorption capability by introducing MgO onto the surface of the $\gamma\text{-Al}_2\text{O}_3$ adsorbent, varying the MgO content from 5% to 15%. Characterization of the adsorbent involves employing X-ray diffraction (XRD), scanning electron microscopy (SEM), infrared spectroscopy (FTIR), surface area measurement (BET), and isoelectric point measurement. Furthermore, the study explores the influence of pH, adsorption time, and adsorbent mass on the Pb^{2+} ion adsorption process using the synthesized materials. Detailed investigation into the adsorption mechanism and kinetics is conducted based on the Langmuir model.

2. Experiments

2.1. Chemicals

Aluminum Nitrate Nonahydrate ($\text{Al}(\text{NO}_3)_3 \cdot 9\text{H}_2\text{O}$); Citric acid; Magnesium nitrate ($\text{Mg}(\text{NO}_3)_2$); Sodium hydroxide (NaOH). All chemicals were supplied by Aladdin Bio-Chem Technology Co., Ltd. and were of analytical purity, with no further purification required.

2.2. Synthesis of $\gamma\text{-Al}_2\text{O}_3$ and $\gamma\text{-Al}_2\text{O}_3@ \text{MgO}$ materials

The $\gamma\text{-Al}_2\text{O}_3$ material was synthesized utilizing the sol-gel technique, employing citric acid as a chelating agent, followed by high-temperature combustion and calcination. Initially, a mixture of 0.1 moles of $\text{Al}(\text{NO}_3)_3 \cdot 9\text{H}_2\text{O}$ and citric acid in a 1:1 molar ratio was stirred in 100 ml of deionized water. The solution was maintained at 80°C for 2 hours to facilitate water evaporation and gel formation. The resulting highly viscous gel was then subjected to 120°C for 16 hours, transforming it into an aerogel state. This aerogel was subsequently sintered in an oven at 900°C for 2 hours to yield nanocrystals with an active surface.

For the synthesis of the $\gamma\text{-Al}_2\text{O}_3@ \text{MgO}$ composite, a co-precipitation method was employed to deposit MgO onto the surface of $\gamma\text{-Al}_2\text{O}_3$. In this process, 1 g of $\gamma\text{-Al}_2\text{O}_3$ material was dispersed using ultrasound for 30 minutes, after which the appropriate amount of $\text{Mg}(\text{NO}_3)_2$ was added to achieve mass ratios of $\gamma\text{-Al}_2\text{O}_3@ \text{MgO}$ at 5%, 10%, and 15%. The mixture was vigorously stirred for 4 hours. Subsequently, a solution containing 100 ml of 0.1 M NaOH was added dropwise to the mixture to precipitate Mg^{2+} ions completely. The resultant precipitate was filtered, washed with distilled water until reaching a pH of 7, and then dried at 100°C for 5 hours. Finally, the sample was calcined at 500°C for 2 hours to crystallize the $\gamma\text{-Al}_2\text{O}_3@ \text{MgO}$ composite. The synthesized samples, denoted as AL, AM5, AM10, and AM15, represent $\gamma\text{-Al}_2\text{O}_3$, $\gamma\text{-Al}_2\text{O}_3@ \text{MgO}$ composite with 5%, 10%, and 15% MgO content, respectively.

2.3. Material characterizations

The crystal structure, morphology and composition of the materials were determined using X-ray diffraction (XRD Bruker D8) with λ ($\text{Cu K}\alpha_2$) = 1.54 Å, scanning electron microscopy (SEM, SM-6510LV) equipped with X-ray energy dispersive spectroscopy (EDS).

To gain insight into the thermal properties of the as-prepared materials, thermal analyses were performed using the TGA Pyris 6. The infrared spectrum (IR) of the

samples was recorded utilizing the Perkin Spectrum Two FT-IR Spectrometer employing the Attenuated Total Reflection (ATR) scattering method. The specific surface area of the materials was measured by BET (Brunauer-Emmett-Teller) method, utilizing the Nova 2000e.

2.4. Study of Pb adsorption using γ -Al₂O₃ and γ -Al₂O₃@MgO materials

2.4.1. Investigation of Isoelectric Point

To investigate the isoelectric point, 0.01 M NaCl solutions were prepared. The pH of these solutions was incrementally adjusted from 2 to 12 using NaOH or HCl. The pH levels were measured using a pH meter. For each sorbent materials, 0.025 g of the as-prepared materials (AL, AM5, AM10 or AM15) was added in to a beaker. Subsequently, 10 ml of the pH-adjusted NaCl solution was added to the material, followed by 30 minutes of sonication and 6 hours of stabilization. After the addition of the sorbent materials, the pH of the solution was measured again. The difference in pH before and after adding the material was compared to the initial pH, revealing the isoelectric point of the sample.

2.4.2. pH-dependent adsorption investigation

For the examination of the pH influence on the adsorption process, 3 mg of the material was dispersed in 200 ml of a Pb(NO₃)₂ solution with a concentration of 12.5 mg/l. This dispersion was performed in an ultrasonic bath for 30 minutes, covering a pH range from 3 to 10. The mixture was stirred for 2 hours, followed by the filtration of the adsorbent. The remaining solution's Pb²⁺ concentration was determined using the ICP-OES method.

2.4.3. Time-dependent adsorption investigation

To analyze the adsorption process over time, 3 mg of AL and AM5, AM10 and AM15 were dispersed in 200 ml of a Pb(NO₃)₂ solution with a concentration of 12.5 mg/l. Ultrasonic dispersion was conducted for 30 minutes at the optimal pH. The mixture was then subjected to continuous magnetic stirring. At 30-minute intervals, the Pb²⁺ concentration in the solution was measured. This monitoring process was extended up to 960 minutes. The concentration of Pb²⁺ was determined through the ICP-OES method.

3. Results and discussions

3.1. Structural and morphological characterization

In the sol-gel reaction, precise control of temperatures during aerogel formation, gel combustion, and sample heating emerges as a critical factor influencing crystal

structure and surface properties. Therefore, to delve deeper into the precise temperatures required for aerogel combustion and calcination, we employed a thermal analysis methodology to study the combustion and calcination processes within the initial gel sample. Fig. 1 illustrates the thermal profiles of the aerogels corresponding to AL and AM10 samples.

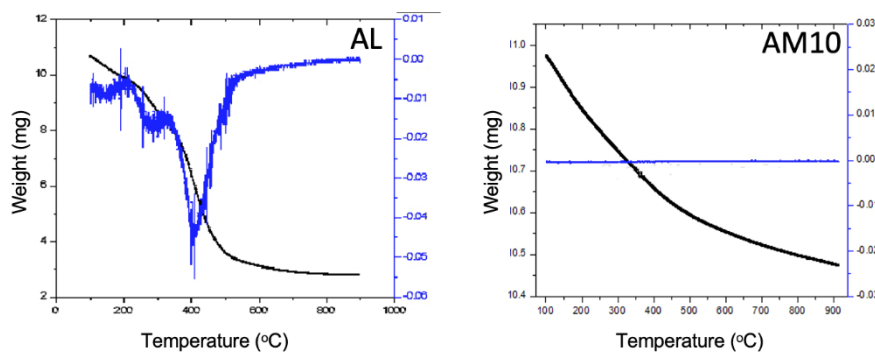


Fig. 1. Thermal analysis diagram of AL and AM10 aerogels.

In the case of the AL aerogel sample, a significant reduction in sample mass is observed within the temperature range of 100 - 400°C. This reduction is attributed to the oxidation of nitrate groups, occurring alongside the oxidation of organic groups to form carbon, which results the liberation of various gaseous components. Additionally, the differential dm/dT curve reveals a distinct peak at 400°C, indicating the peak combustion rate. Consequently, the gel combustion temperature was judiciously selected as 400°C. Within the temperature span of 600 - 900°C, gradual volumetric changes are observed, with a notable plateau emerging between 800 - 900°C. This temperature range serves to ensure complete incineration of any residual carbon and remaining organic substances, facilitating the crystallization of γ - Al_2O_3 . Hence, a temperature of 900°C was a chosen for this purpose.

Regarding the AM10 aerogel sample, thermal analysis conducted within the temperature range of 100 - 500°C demonstrates a decreasing sample mass, coinciding with the dehydration process transitioning from $\text{Mg}(\text{OH})_2$ to MgO . This mass reduction exhibits a continuous and steady decline, with no discernible decomposition point on the differential curve. Consistent with prior research findings, a temperature of 500°C was selected for the crystallization of MgO . This temperature was sustained for a duration of 2 hours, yielding the following reaction:



To assess the successful fabrication of the materials, an analysis of the crystal structure is conducted through X-ray diffraction (XRD). The XRD patterns of the experimental samples elucidate the crystallographic characteristics of the absorbent materials. Refer to Fig. 2 for the X-ray diffraction diagrams showcasing the crystal structure of the as-prepared materials.

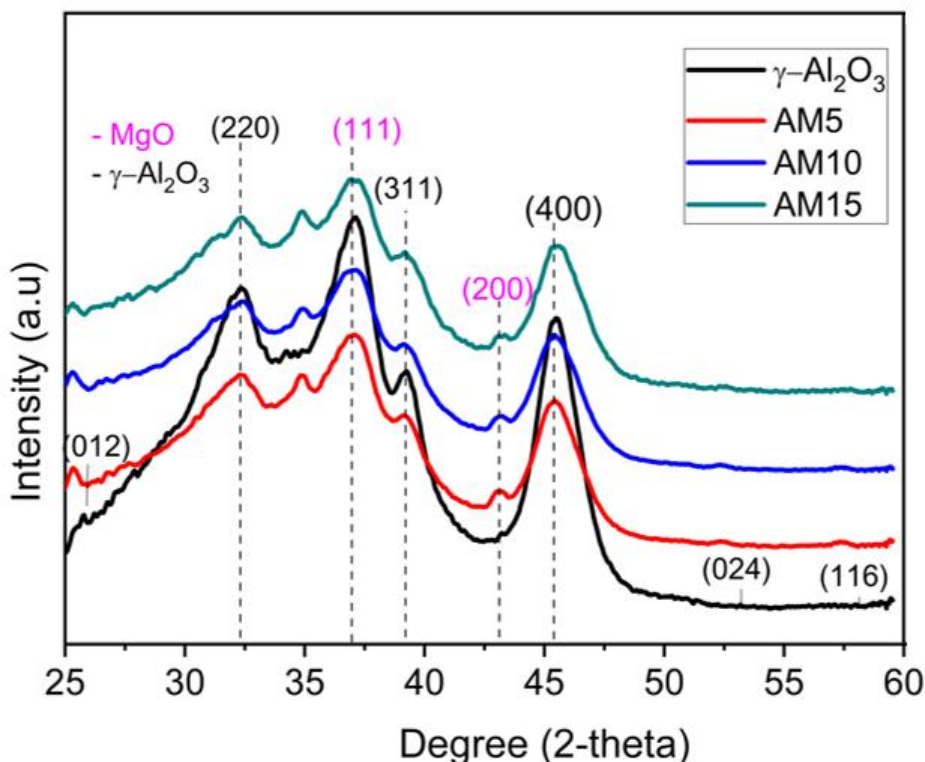


Fig. 2. XRD diffraction patterns of as-prepared sorbent material samples AL, AM5, AM10 and AM15.

The X-ray diffraction (XRD) pattern of the AL sample distinctly reveals a tightly packed cubic crystal structure. The diffraction peaks (220), (311), (222), and (400) corresponding to diffraction angles $2\theta = 32.1^\circ$, 37.6° , 39.3° , and 45.70° , respectively, are characteristic peaks of the $\gamma\text{-Al}_2\text{O}_3$ crystal (ICDD-PDF 00-010-0425). Upon the introduction of MgO onto the surface of Al_2O_3 , the additional distinctive peaks of MgO appear in the XRD patterns of the AM5, AM10, and AM15 samples (ICDD-PDF No. 87-0653). The diffraction peaks at $2\theta = 36.9^\circ$ and 42.90° correspond to characteristic peaks of MgO, aligning with the (111) and (200) diffraction planes of the cubic crystal structure. The broadening of these peaks also indicates the initially small crystallite size of the hybrid materials.

The size and morphological attributes of γ -Al₂O₃ nanoparticles, following calcination at 900°C for a duration of 2 hours, are depicted in Fig. 3 through scanning electron microscopy (SEM) imaging, acquired at different magnification. The SEM images reveal prevailing spherical shape for the particles, characterized by the brighter, whereas the pores within the structure appear darker in color. The findings underscore the effectiveness of the sol-gel method in generating AL samples characterized by a size distribution ranging from 12 to 50 nm. Notably, the particles within these samples display isotropic growth, resulting in a predominantly spherical and uniform morphology.

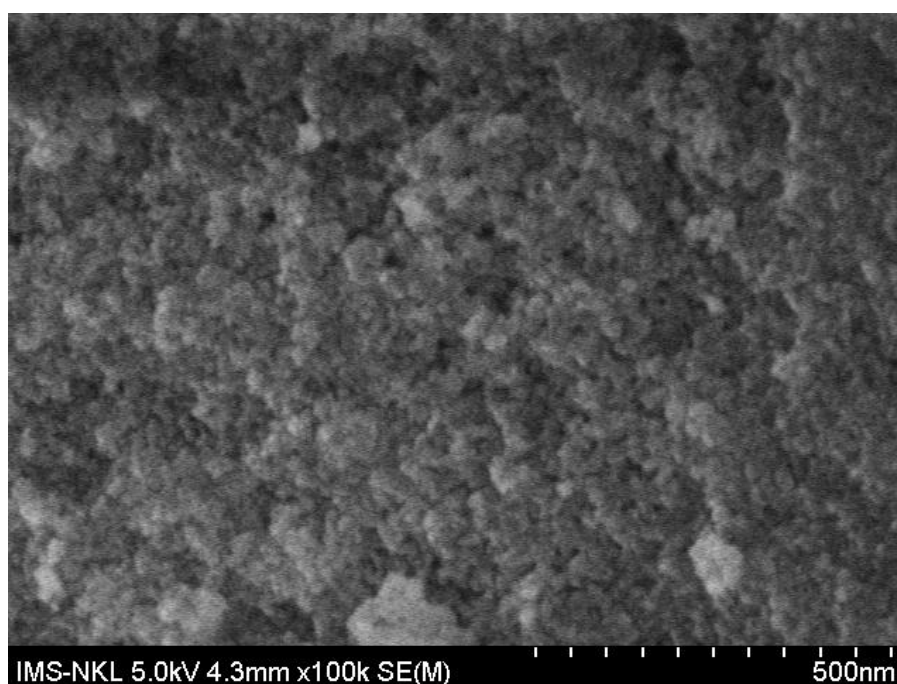


Fig. 3. The SEM images of AL sample synthesized by sol-gel method.

Chemical elemental composition analysis of the adsorbent sample was conducted using X-ray Energy Dispersive Spectroscopy (EDX) and Fig. 4 presented comprehensive elemental composition of AL and AM10 samples. The result showed that AL sample comprises of oxygen (O) and aluminum (Al) atoms with the atomic ratio of aluminum (Al) and oxygen (O) within the sample aligns with the composition characteristic of Al₂O₃ crystals. Meanwhile, the EDX spectrum of the AM10 adsorbent sample reveals the presence of Mg, O and Al atoms, where the mass percentage of MgO within AM10 was determined to about 9%. This proportion closely approximates the original synthesizing composition, providing compelling evidence that the majority of MgO ions have been effectively integrated into the Al₂O₃ adsorbent material.

The surface properties of adsorbent materials play a crucial role in determining their ion adsorption capacity. Consequently, the investigation into specific surface area and surface properties was undertaken using the Brunauer-Emmet-Teller (BET) method, isoelectric point determination, and FTIR infrared spectroscopy. The surface areas (S) for samples AL and AM10 were found to be $S_{AL} = 166,817 \text{ m}^2/\text{g}$ and $S_{AM10} = 142,586 \text{ m}^2/\text{g}$, respectively. Notably, the introduction of MgO led to a reduction in the surface area of the starting material. This decrease may be attributed to MgO having a lower specific surface area compared to Al_2O_3 . In accordance with prior research [4], the impact of MgO on specific surface area tends to be consistent with an increase in MgO content, resulting in a reduction in specific surface area. The authors of previous work explained that the addition of MgO likely diminishes the volume of certain surface pores in Al_2O_3 by filling these pores during the fabrication process, potentially forming some surface oxides through reactions during sample calcination.

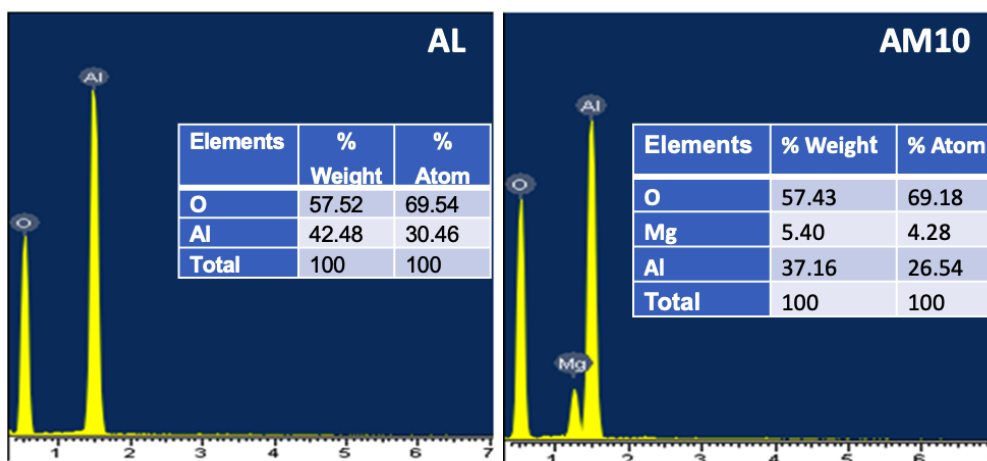


Fig. 4. EDS analysis of AL and AL10 samples.

Furthermore, FTIR infrared spectra were examined for various samples, including AL1 (hydrated $\gamma\text{-Al}_2\text{O}_3$), AL2 (hydrated $\gamma\text{-Al}_2\text{O}_3$ subjected to ultrasound and subsequently dried at 120°C for 1.5 hours), and $\gamma\text{-Al}_2\text{O}_3\text{@MgO}$ series including AM5, AM10, AM15, subjected to ultrasound and dried at 1200°C for 1.5 hours. The results, as depicted in Figure 5, elucidate the distinct surface hydration and non-hydration states of the adsorbent samples.

The FTIR spectrum showing the absorption region between $400 - 450 \text{ cm}^{-1}$ reveals the presence of Al–O–Al bonds, indicative of Al_2O_3 within the sample. Peaks observed

at 1364.08 and 1368.06 cm^{-1} signify the emergence of Mg-O bonds in both MgO and $\text{Mg}(\text{OH})_2$ [5]. Notably, samples AL1 and AL2 exhibit similar absorption spectra.

In contrast, samples AM5, AM10, and AM15, upon drying at 120°C , display increased absorbance within the range of 3388.50 - 3394.08 cm^{-1} and the emergence of a broad peak. This broad peak is characteristic of O-H bonding, attributed to the hydration of Mg^{2+} ions on the material's surface. These findings suggest that samples containing MgO exhibit higher surface basicity when dispersed in water compared to $\gamma\text{-Al}_2\text{O}_3$ samples.

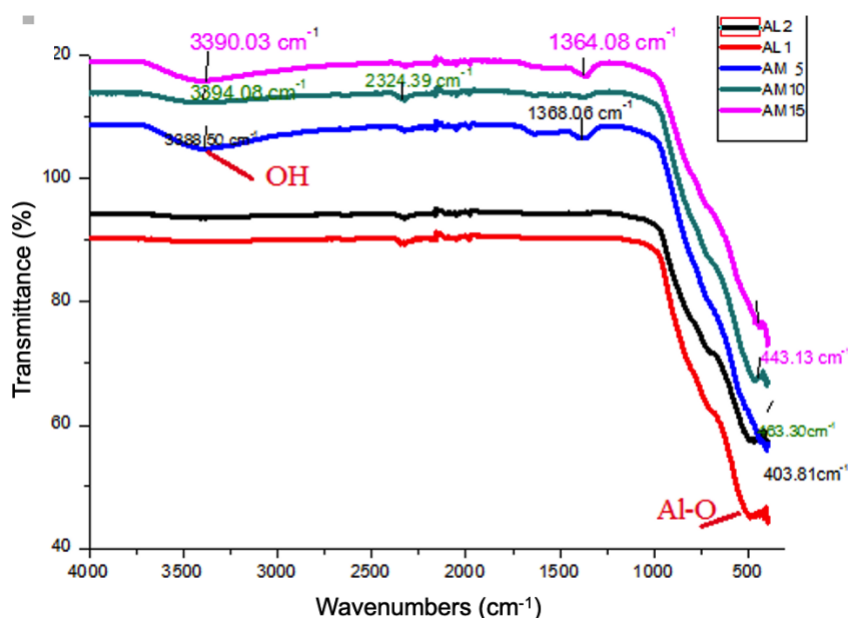


Fig. 5. FTIR spectra of AL1, AL2, AM, AM10 and AM15 samples.

The measurement of the isoelectric point (IEP) elucidates the surface charge of the material at various pH levels and identifies the point at which the material's surface becomes electrically neutral. IEP plays a critical role in determining the pH at which the material's metal ion adsorption process occurs. The IEP values and the corresponding pH changes (ΔpH) in the solution upon the addition of adsorbent materials AL, AM5, AM10, and AM15 are illustrated in Figure 6. The IEP value for AL was determined at $\text{pH} = 6.5$, while the introduction of MgO into $\gamma\text{-Al}_2\text{O}_3$ has indeed led to increase of IEP value to $\text{pH} = 7.4$, 7.6 and 8.0 for AM5, AM10 and AM15, respectively. This upward shift in the IEP towards higher pH values indicates the enhanced surface properties enriched with -OH groups of the adsorbent material upon the addition of MgO.

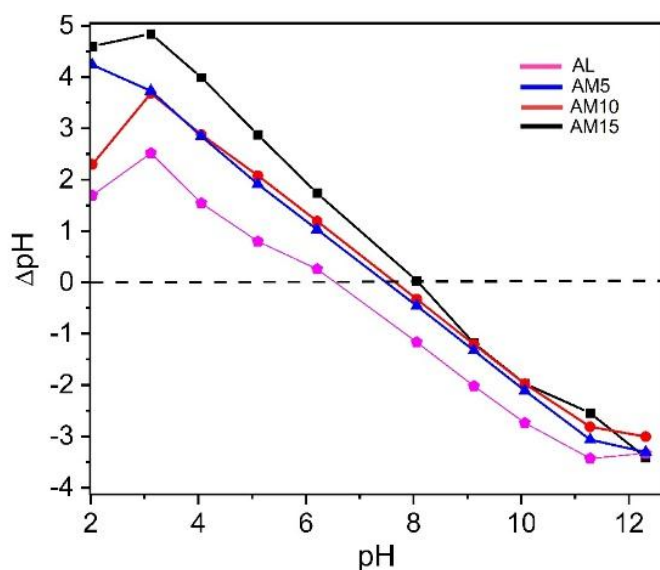


Fig. 6. The plot of isoelectricpoint at different pH of AM, AM5, AM10 and AM15 samples.

3.2. Investigation of the adsorption process of Pb^{2+} ions by $\gamma-Al_2O_3@MgO$

a) pH optimization

Optimizing the initial pH value of the adsorption process is a crucial step that significantly impacts the adsorption capacity for heavy metal ions. The initial concentration of the lead in this particular study is 12.5 mg/L. Of note, when pH of solution becomes more and more basic, the treatment process primarily involves the precipitation of Pb^{2+} ions rather than adsorption. Therefore, the investigated pH range was maintained below 11. Fig. 7 shows the effect of pH on the adsorption efficiency (H%). For AM sample, the adsorption capacity reached a peak at pH = 7, then decline when increasing pH, the pH was over 9, the H% values became slightly higher and remained stable due to the precipitation of Pb^{2+} ions. Meanwhile, for AL, the H% was high at the pH range of 7 - 8, before decreasing when pH shifting toward 10. At pH = 11, the calculated H% was increased dramatically due to the precipitation of Pb^{2+} ions. Notably, the adsorption efficiency of the sample containing 10% MgO surpasses that of the $\gamma-Al_2O_3$ sample under identical adsorption conditions, affirming the efficacy of MgO in the Pb adsorption process. Based on these results, for the next adsorption experiments, the optimum pH value of 7 was selected for both AL and AM series.

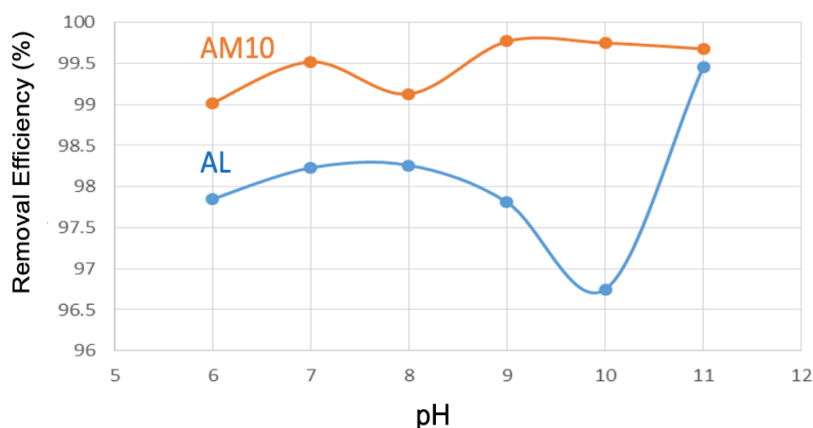


Fig. 7. The influence of pH on the adsorption efficiency.

b) Adsorption kinetics and isotherm

The effect of time on the adsorption of Pb^{2+} ions by sorbent materials AL, AM5, AM10, AM15 was studied at the optimal pH value of 7 with an adsorption time of 8 hours. The results indicate that the adsorption process shows a good fit with the pseudo-second-order adsorption equation [19]:

$$\frac{t}{q_t} = \frac{1}{k_2 q_e^2} + \frac{t}{q_e}$$

where k_2 is reaction rate constant ($g/mg \cdot time$); q_e , q_t are adsorption capacity at equilibrium and time t (mg/g). The fitted model applied for AL and AM10 samples shown in Fig. 8a-b. As a result, the equilibrium adsorption concentration (q_e) values were calculated for these samples (see Table 1).

For finding maximum adsorption capacity, the Langmuir isotherm model [19] was employed:

$$\frac{C}{q} = \frac{1}{K_L \cdot q_{max}} + \frac{1}{q_{max}} C$$

where q is equilibrium adsorption capacity (mg/g); q_{max} is maximum adsorption capacity (mg/g); C is concentration of adsorbent at equilibrium (mg/L); K_L is Langmuir constant (L/mg). The initial concentrations of Pb^{2+} ions used in this study varied from 7.5 mg/L to 22.5 mg/L . The maximum adsorption capacities determined from Langmuir model for AL, AM5, AM10 and AM15 were 135, 137, 145 and 141 mg/g , respectively. This result suggests that as the MgO concentration increases, so does the lead absorption capacity. The reason is that the presence of MgO leads to the increase of OH⁻ group on the surface,

which subsequently increased the number of adsorption centers. However, as MgO content reached 15%, the adsorption capacity was decreased. It is because the excessive MgO results in a reduction in the specific surface area of Al₂O₃, thereby diminishing the adsorption process.

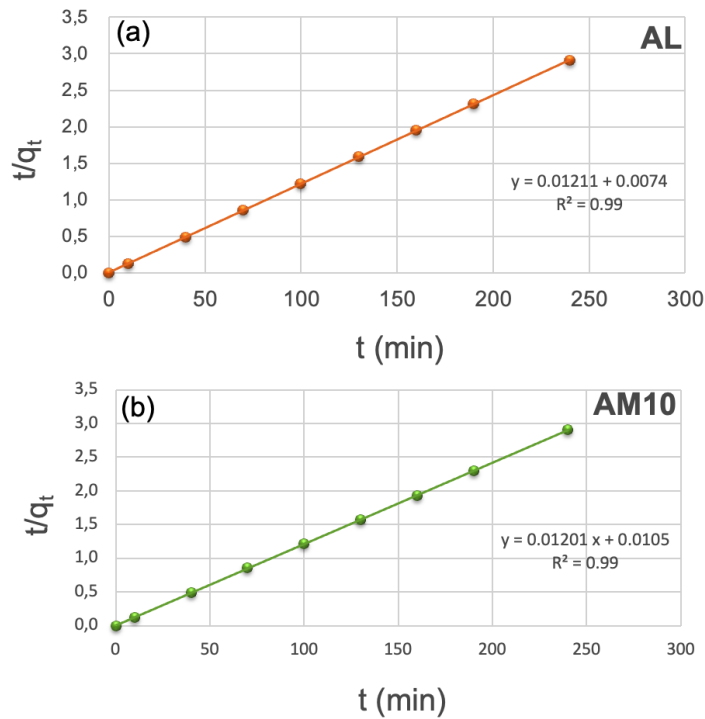


Fig. 8. The plot of t/q_t vs t of (a) AL and (b) AM10 samples.

Table 1. Parameters (R^2 , q_e , and k) in the adsorption kinetic equation

Sample	R^2	q_e (mg/g)	k (g/mg.min ⁻¹)
AL	0.99	82.57	0.024
AM5	0.99	82.71	0.029
AM10	0.99	83.26	0.026
AM15	0.99	83.06	0.032

In conclusion, γ -Al₂O₃ is a porous material with a substantial surface area and active surface sites capable of adsorbing heavy metal ions. However, surface modification further enhances adsorption capacity, augmenting the advantages of a large specific surface area. MgO effectively boosts the surface adsorption capacity of γ -Al₂O₃ while preserving the material's large specific surface area. The mechanism illustrates that MgO

enhances surface basicity [20], facilitating the adsorption of heavy metal ions. With high adsorption efficiency in a neutral environment, this material demonstrates the potential for chemical-free processing and adsorbent reuse.

4. Conclusion

In this study, γ -Al₂O₃ nanomaterials were successfully synthesized with a specific surface area of 166,817 m²/g using the citrate sol-gel method. Additionally, MgO particles were introduced onto γ -Al₂O₃ with varying components ranging from 5% to 15% by weight. Modern physicochemical analysis techniques (including FT-IR, SEM, EDX, and PZC) were employed to elucidate the crystal structure and composition of both γ -Al₂O₃ and γ -Al₂O₃@MgO composites, confirming the presence of MgO within the crystalline phase on the γ -Al₂O₃ surface and the occurrence of surface hydration on the oxide material.

Furthermore, the investigation into the adsorption capacity of Pb²⁺ ions on the synthesized adsorbent materials revealed that the optimal conditions for Pb²⁺ adsorption occurred at pH 7 and a contact time of 960 minutes. Enhanced adsorption efficiency was observed, with AM10 displaying the highest adsorption capacity, reaching a maximum Pb²⁺ adsorption capacity of 145 mg/g. The adsorption of Pb²⁺ ions on these adsorbent materials adhered to the Langmuir isotherm adsorption model, and the adsorption process followed the second-order adsorption kinetic model. The proposed enhanced adsorption mechanism is attributed to MgO, which introduces basicity to the surface of the adsorbent.

References

- [1] S. Mitra et al., "Impact of heavy metals on the environment and human health: Novel therapeutic insights to counter the toxicity," *Journal of King Saud University - Science*, Vol. 34, Iss. 3, 2022, 101865.
- [2] M. Jaishankar et al., "Toxicity, mechanism and health effects of some heavy metals," *Interdiscip Toxicol*, Vol. 7, No. 2, pp. 60-72, 2014.
- [3] A. Pohl, "Removal of Heavy Metal Ions from Water and Wastewaters by Sulfur-Containing Precipitation Agents," *Water, Air, & Soil Pollution*, Vol. 231, Iss. 10, 2020, 503.
- [4] F. M. Pang et al., "Removal of lead, zinc and iron by coagulation-flocculation," *Journal of the Taiwan Institute of Chemical Engineers*, Vol. 42, Iss. 5, pp. 809-815, 2011.
- [5] R. Arora, "Adsorption of Heavy Metals - A Review," *Materials Today: Proceedings*, Vol. 18, pp. 4745-4750, 2019.
- [6] M. Z. Zaimee, M. S. Sarjadi, and M. L. Rahman, "Heavy Metals Removal from Water by Efficient Adsorbents," *Water*, Vol. 13, Iss. 19, 2021. DOI: 10.3390/w13192659

- [7] N. A. A. Qasem, R. H. Mohammed, and D.U. Lawal, "Removal of heavy metal ions from wastewater: a comprehensive and critical review," *npj Clean Water*, Vol. 4, No. 1, 2021, 36.
- [8] P. Miretzky, A. Saralegui, and A. Fernández Cirelli, "Simultaneous heavy metal removal mechanism by dead macrophytes," *Chemosphere*, Vol. 62, No. 2, pp. 247-254, 2006.
- [9] A. E. Burakov et al., "Adsorption of heavy metals on conventional and nanostructured materials for wastewater treatment purposes: A review," *Ecotoxicology and Environmental Safety*, Vol. 148, pp. 702-712, 2018.
- [10] D. S. Malik, C. K. Jain, and A. K. Yadav, "Removal of heavy metals from emerging cellulosic low-cost adsorbents: A review," *Applied Water Science*, Vol. 7, No. 5, pp. 2113-2136, 2017.
- [11] N. S. Topare and V. S. Wadgaonkar, "A review on application of low-cost adsorbents for heavy metals removal from wastewater," *Materials Today: Proceedings*, Vol. 77, pp. 8-18, 2023.
- [12] S. S. Kolluru et al., "Heavy metal removal from wastewater using nanomaterials-process and engineering aspects," *Process Safety and Environmental Protection*, Vol. 150, pp. 323-355, 2021.
- [13] C. Liosis et al., "Heavy Metal Adsorption Using Magnetic Nanoparticles for Water Purification: A Critical Review," *Materials*, Vol. 14, 2021. DOI: 10.3390/ma14247500
- [14] M. Karnib et al., "Heavy Metals Removal Using Activated Carbon, Silica and Silica Activated Carbon Composite," *Energy Procedia*, Vol. 50, pp. 113-120, 2014.
- [15] M. G. Ghoniem et al., "Efficient and Rapid Removal of Pb(II) and Cu(II) Heavy Metals from Aqueous Solutions by MgO Nanorods," *Inorganics*, Vol. 10, 2022. DOI: 10.3390/inorganics10120256
- [16] Y. Wei et al., "Enhanced lead and copper removal in wastewater by adsorption onto magnesium oxide homogeneously embedded hierarchical porous biochar," *Bioresource Technology*, Vol. 365, 2022, 128146.
- [17] A. Rahmani, H. Z. Mousavi, and M. Fazli, "Effect of nanostructure alumina on adsorption of heavy metals," *Desalination*, Vol. 253, No. 1, pp. 94-100, 2010.
- [18] F. Ezati, E. Sepehr, and F. Ahmadi, "The efficiency of nano-TiO₂ and γ -Al₂O₃ in copper removal from aqueous solution by characterization and adsorption study," *Scientific Reports*, Vol. 11, No. 1, 2021, 18831.
- [19] A. S. Poursani, A. Nilchi, A. H. Hassani, M. Shariat, and J. Nouri, "A novel method for synthesis of nano- γ -Al₂O₃: Study of adsorption behavior of chromium, nickel, cadmium and lead ions," *International Journal of Environmental Science and Technology*, Vol. 12, No. 6, pp. 2003-2014, 2015. DOI 10.1007/s13762-014-0740-7
- [20] Shahriar Mahdavi, Mohsen Jalali & Abbas Afkhami, *Heavy metals removal from aqueous solutions using TiO₂, MgO, and Al₂O₃ nanoparticles*, *Chemical Engineering Communications*, 2013, pp. 448-470.

TỔNG HỢP VÀ KHẢO SÁT ĐẶC TÍNH CỦA $\gamma\text{-Al}_2\text{O}_3\text{@MgO}$ ỨNG DỤNG CHO HẤP PHỤ Pb TRONG DUNG DỊCH

Nguyễn Kim Thanh^a, Nguyễn Thị Lan Anh^a, Dương Minh Tuấn^a,
Phạm Việt Linh^a, Lê Thị Vinh Hạnh^a, Trần Vũ Sinh^a, Hà Văn Hào^a, Lê Thế Sơn^a

^aKhoa Hóa - Lý kỹ thuật, Trường Đại học Kỹ thuật Lê Quý Đôn

Tóm tắt: Nghiên cứu này tập trung vào việc nâng cao khả năng hấp phụ cho các ion chì bằng cách đưa MgO lên bề mặt $\gamma\text{-Al}_2\text{O}_3$, tạo thành $\text{Al}_2\text{O}_3\text{@MgO}$. Các hạt nano $\gamma\text{-Al}_2\text{O}_3$ được tổng hợp bằng phương pháp sol-gel trên mẫu citrate. MgO được tích hợp lên bề mặt của các hạt nano $\gamma\text{-Al}_2\text{O}_3$, với nồng độ MgO khác nhau (5%, 10% và 15% trọng lượng). Các phát hiện chỉ ra rằng cả hai pha tinh thể $\gamma\text{-Al}_2\text{O}_3$ và MgO đều có cấu trúc lập phương (nhóm đối xứng Fd3m), được hình thành trong mẫu. Mặc dù diện tích bề mặt riêng giảm từ 166 m²/g xuống 135 m²/g, độ bazơ bề mặt tăng tỉ lệ thuận với lượng MgO đưa vào mẫu. Ảnh hưởng của các điều kiện hấp phụ khác nhau như pH, khối lượng chất hấp phụ và thời gian tiếp xúc đến khả năng hấp phụ ion Pb²⁺ đã được kiểm tra có hệ thống. Điều kiện tối ưu (pH = 7, thời gian hấp phụ 8 giờ) cho thấy vật liệu $\gamma\text{-Al}_2\text{O}_3$ chứa 10% MgO tính theo trọng lượng cho khả năng hấp phụ Pb²⁺ cao nhất ở mức 145 mg/g, vượt qua khả năng hấp phụ 135 mg/g của vật liệu $\gamma\text{-Al}_2\text{O}_3$.

Từ khóa: $\gamma\text{-Al}_2\text{O}_3\text{@MgO}$; hấp phụ Pb²⁺; tính bazơ bề mặt.

Received: 12/09/2023; Revised: 20/10/2023; Accepted for publication: 17/11/2023

